ISSN 0915-633X

NATIONAL INSTITUTE FOR FUSION SCIENCE

Analytical Model of Neutral Gas Shielding for Hydrogen Pellet Ablation

Boris V. Kuteev and Lev D. Tsendin

(Received - Oct. 10, 2001)

NIFS-717 Nov. 2001

This report was prepared as a preprint of work performed as a collaboration reserch of the National Institute for Fusion Science (NIFS) of Japan. This document is intended for infomation only and for future publication in a journal after some rearrangements of its contents.

Inquiries about copyright and reproduction should be addressed to the Research Information Center, National Institute for Fusion Science, Oroshi-cho, Toki-shi, Gifu-ken 509-02 Japan.

RESEARCH REPORT
NIFS Series

TOKI, JAPAN

Analytical Model of Neutral Gas Shielding for Hydrogen Pellet Ablation

Boris V. KUTEEV, LEV D. TSENDIN

State Technical University, St. Petersburg 195251, RUSSIA
National Institute for Fusion Science, Toki, Gifu 509-5292, JAPAN

e-mail: kuteev@phtf.stu.neva.ru

Keywords: pellet, ablation, model, neutral gas shielding, gas dynamics, scaling.

Abstract:

A kinetic gasdynamic scaling for hydrogen pellet ablation is obtained in terms of a neutral gas shielding model using both numerical and analytical approaches. The scaling on plasma and pellet parameters proposed in the monoenergy approximation by Milora and Foster $dR_{pe}/dt \sim S_n^{2/3} R_p^{-2/3} q_{eo}^{1/3} m_i^{-1/3}$ is confirmed. Here R_p is the pellet radius, S_n is the optical thickness of a cloud, q_{eo} is the electron energy flux density and m_i is the molecular mass. Only the numeral factor is approximately two times less than that for the monoenergy approach. Due to this effect, the pellet ablation rates, which were obtained by Kuteev on the basis of the Milora scaling, should be reduced by a factor of 1.7. Such a modification provides a reasonable agreement (even at high plasma parameters) between the two-dimensional kinetic model and the one-dimensional monoenergy approximation validated in contemporary tokamak experiments. As the cloud (in the kinetic approximation) is significantly thicker than that for the monoenergy case as well as the velocities of the gas flow are much slower, the relative effect of plasma and magnetic shielding on the ablation rate is strongly reduced.

1 Introduction

The problem of hydrogen pellet ablation in high temperature plasmas has been analyzed by numerous investigators (see [1,2] and references) as one strongly relevant to a tokamak reactor fuelling. It is generally accepted now that the ablation mechanism consists in solid hydrogen sublimation under influence of heat flux, which is supplied mainly by electrons of the hot ambient plasma. Due to the extremely low value of sublimation energy and high-energy fluxes in tokamak plasmas, a dense cloud of ablatant surrounds the pellet, and the incoming heat flux is almost completely screened at the pellet surface. In the pellet vicinity, the expanding neutral molecular hydrogen gas produces this shielding. At larger distances, ionization occurs and an additional shielding appears being produced by the cold outflowing plasma cloud, which expands almost one-dimensionally along the magnetic field [3]. Along with the magnetic field distortion, electrostatic fields at the pellet surface and in the plasma cloud result in additional reduction of the incoming heat flux (electrostatic [4] and magnetic shielding [5,6]).

The neutral gas shielding model (NGSM) treats the interaction between the flux of fast plasma electrons and the expanding neutral cloud. It was first proposed in [7,8], see also [9-11]. This part of the pellet ablation problem seems at present to be the most advanced and detailed. In Ref. [7,8] a self-consistent one-dimensional model was analyzed, in which expansion and acceleration of the molecular hydrogen cloud was produced by heating due to primary electrons approximated as a monoenergy beam. It was pointed out that the gas dynamic flow of the cloud is subsonic at the pellet surface and supersonic at infinity. The flow characteristics are determined by the condition of smooth transition through the sonic point. This means that the cloud properties depend substantially on the distribution of the heat sources. The calculations made in Ref. [7], where the energy deposition in the cloud was considered as uniform and the finite boundary conditions of the cloud temperature T, velocity V, and Mach

number M at the pellet surface were imposed, and in Ref. [8] using a more realistic gas heating model but the zero boundary conditions for T, V, M, gave practically coincident values for the ablation rate. A more precise analysis of elementary processes in the cloud [11] did not affect these values considerably.

A characteristic feature of energy flux penetration through a cloud is an almost complete shielding of the incoming electron energy flux, so that the heat flux at the pellet surface is by orders of magnitude less than in undisturbed plasma. Due to higher energy losses for lower electron energy range, the heat flux close to a pellet is determined by a tail of the undisturbed electron distribution function EDF and the problem is essentially of kinetic nature. The ablation rate depends crucially on the shape of the EDF on the pellet surface. Due to the complex interaction of the fast primary electrons with the expanding cloud, this EDF is considerably different from the undisturbed one at the infinity, which is determined by properties of the ambient plasmas. For such a reality, the monoenergy approximation of Ref. [7,8] seems to be too rough. Instead of the thermal electrons, the shielding must be calculated with respect to the high energy electrons of the EDF tail, as it was considered in Ref. [15]. Therefore, one may neglect the primary electrons' scattering (see Ref. [15] for arguments) and apply to them the approximation of continuous energy losses. The problem reduces then to motion of electrons along the magnetic lines under the influence of velocity-dependent retarding force $L(v)$. Since $L(E)$ decreases with the electron energy E, the ablation cloud is far more transparent for the fast electrons than for the thermal ones. In the case $L(E)$=Const, the EDF at the pellet surface coincides with the unperturbed one, which is shifted by the electron energy loss ΔE along the trajectory. The ΔE value is determined by the shielding and it depends parametrically on the azimuthal angle α on the surface. The EDF, which is Maxwellian at the infinity, remains also Maxwellian at the pellet in this case. But the realistic decreasing dependence $L(E)$ results in a distortion of the EDF shape. It becomes more enriched by the high energy electrons than the undisturbed one and its "effective temperature" (or average energy) rises. Although the kinetic effects described above have been formulated and taken into account, the rough assumption about sonic flow anywhere inside the cloud was used in Ref. [15], so the resulting ablation rates were overestimated.

On the other hand, the energy supply to the cold dense gas, which is responsible for the main shielding inside the cloud, is also determined by fast rather than the thermal part of the undisturbed EDF. This fact results in a considerable varying the spatial distribution of the energy deposition inside the cloud. In the pellet vicinity the energy supply is much lower than that for the monoenergy approximation. This is mainly due to the fact that the effective mean electron energy for the Maxwellian EDF remains of the order of undisturbed electron temperature, and the particle flux decreases exponentially, while for the monoenergy approximation the particle flux is conserved (or slightly reduced by electron scattering), and the mean electron energy is low close to the pellet surface. This determines substantial distinctions of the cloud densities and velocities. Thus, the neglect of the electron kinetics influence on the gas dynamics has led to the overestimated ablation rates in Ref. [10]; see also [17].

Of course, the pellet surface is screened from the incoming electron heat flux not only by the neutral cloud, but also by the expanding cold plasma cloud, by electric field in it, by distortion of magnetic field etc. A most detailed and precise numerical code of the pellet ablation process considering these effects was developed in Ref. [12-14]. In Ref. [12] a comparison between results of different NGS-models and the codes was performed, which gave a surprisingly good agreement between [8,15] and [13,14]. In Ref. [16] the experimental data about the ablation collected in the international database IPADBASE were compared with the NGSM, and also a reasonable agreement was obtained. The fact that the NGSM describes satisfactorily such a crude global characteristic as the ablation rate means simply that with the neutral cloud a considerable part of the total shielding is associated.

For a further development of ablation models and a quantitative comparison of different factors affecting the ablation, it is very significant not only to estimate the ablation rate but also to understand the internal structure of the ablation cloud. Therefore, it is desirable to obtain comparatively simple and, if possible, analytical expressions for the neutral shielding problem in order to use them for designing more complicated models and derivation of more detailed scaling laws. A more detailed experimental information about the shielding process is also very desirable.

In this paper we show that a two-dimensional gas dynamic solution can be obtained for Maxwellian plasma analytically and consider the effect of the kinetic gas dynamics on the ablation rate scaling [10]. Our analysis [17] and the Macaulay calculations, which use the kinetic two-dimensional code [11], have shown that with Maxwellian electrons the subsonic region is broader (sonic radius becomes $\sim 2r_p$ compared to 1.33 for the Milora case [7] and 1.6 for the Parks one [8]), and the neutral shielding grows up. Nevertheless, the region in the vicinity of the pellet remains dominant in the shielding formation. Due to this fact the azimuth gradients in the main part of the cloud are small compared with the radial ones. This allows us to hope that the parametric approach, in which the azimuth derivatives in the fluid equations are neglected and the dependence (parametric) on the azimuth angle α remains only in the source terms and in coefficients of the ordinary differential equations on the radial coordinate, is valid at least for a qualitative description.

The most striking result of taking the electron kinetics into account is the considerably (up to 20 times) higher values of the neutral cloud thickness compared with the monoenergy analysis [7,8]. Due to the lower heating, the gas density

decreases slower with distance from the pellet. Nevertheless, the heat flux transported by fast electrons penetrates through a dense cloud and provides ablation rates close to the monoenergy estimations. The resulting scaling law for the ablation rate differs from that of Ref. [10] only by a factor of 0.6. Higher values of the cloud thickness in the kinetic model considerably raise the contribution of neutral shielding to the total one. In combination with the above-mentioned insensitivity of the ablation rate to the shielding mechanism details this fact seems to explain the surprisingly good correlation of the NGSM predictions with the pellet penetration length data obtained on contemporary tokamaks [9,10,16].

The general equations and numerical results are considered in Section 2. In Section 3 we formulate our analytical approach. In Section 4 the results of the two approaches are discussed and the ablation scaling [10] is corrected. For the sake of simplicity, we neglect here the charging effects, atomic processes in the cloud and assume the flow to be totally molecular, and polytropic.

2 General Equations and Numerical Approach

Consider first the problem as a one-dimensional one. Gasdynamic equations for the ablation cloud have the form [7,8]

$$m_i N V R^2 = G \tag{1}$$

$$m_i N V \frac{dV}{dR} + \frac{d}{dR} NT = 0 \tag{2}$$

$$\frac{G}{R^2}\frac{d}{dR}\left[\frac{\gamma T}{(\gamma-1)m_i} + \frac{V^2}{2}\right] = Q \tag{3}$$

$$Q = Aa(R)N = divq_e = \frac{dq_e}{dz} = \frac{dq_e}{dS_n}\frac{dS_n}{dz} = -\frac{dq_e}{dS_{n0}}\left(\frac{\frac{dq_e}{dS_n}}{\frac{dq_e}{dS_{n0}}}\right)N \tag{4}$$

where m_i is the molecular mass of hydrogen, N is the gas density, V is the gas velocity, R is the radius, $4\pi G = m_i dN/dt$ is the mass ablation rate, γ is the ratio of the specific heats and Q is the heat power density deposited by the electron energy flux q_e incident upon the pellet along the magnetic field parallel to the z-axis.

Here we have used an optical thickness (line density integral) of the cloud

$$S_n(R) = \int_R^\infty N dR \tag{5}$$

and defined the constant

$$A = \frac{dq_e}{dS_{n0}} \tag{6}$$

which is a derivative at infinity of the electron heat flux q_e over the optical thickness S_n. The function

$$a(R) = \left(\frac{dq_e}{dS_n} \Big/ \frac{dq_e}{dS_{n0}}\right) \tag{7}$$

is the dimensionless heating rate per cloud particle, which is equal to 1 at infinity. In the Milora analysis $a(R)=1$ was assumed everywhere. Parks used an expression for the $a(R)$-function close to

$$a(R) = \left(\frac{E(R)}{E_0}\right)^{1/2} \tag{8}$$

where $E_0 = 2T_e$ is the mean electron energy at infinity, and $E(R)$ is the mean electron energy at a point R.

In Maxwellian plasmas, the function $a(S_n)$ has been calculated in [10] for several electron temperatures. A typical dependence $a(S_n)$ for the plasma with T_e=5000 eV and $n_e = 1.6\times10^{14}$ cm^{-3} is shown in Fig. 1 (see [17] for lower parameters). Characteristic is an almost exponential decrease of the $a(S_n)$ with growth of the optical thickness.

If we define the dimensionless radius r normalized by the pellet radius R_p

$$r = R/R_p, \tag{9}$$

the characteristic gas velocity in the cloud as

$$V_0 = \left(\frac{AR_p}{m_i}\right)^{1/3} \tag{10}$$

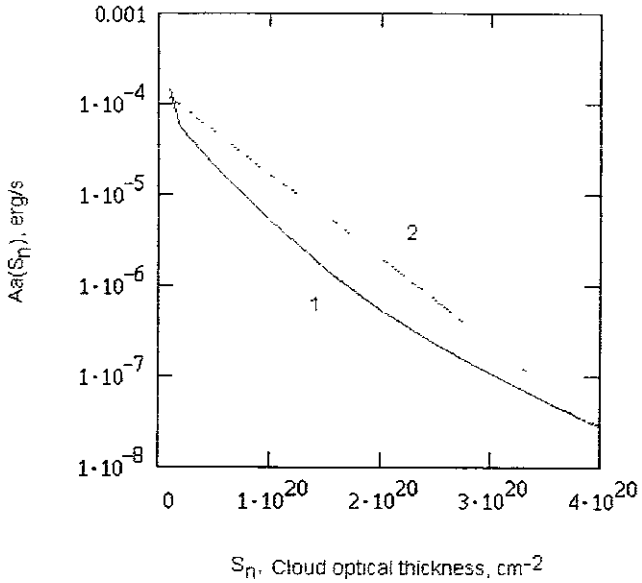

Figure 1: Energy losses per particle in hydrogen cloud versus the cloud optical thickness. The plasma and pellet parameters: T_e=5000 eV, n_e=1.6×10^{14} cm^{-3}, R_p=0.15 cm. 1- numerical dependence obtained with the algorithm of Ref. [10]. 2- approximation used in our numerical analysis of the cloud gas dynamics.

and normalize the gas velocity V and temperature T as follows:

$$v=\frac{V}{V_0}, \qquad \theta=\frac{T}{m_i V_0^2} \tag{11}$$

the set of Eqs. (1)-(4) can be transformed to a dimensionless form

$$\frac{dv}{dr}+r^2\frac{d}{dr}\left(\frac{\theta}{vr^2}\right)=0 \tag{12}$$

$$v\frac{d}{dr}\left(\frac{\gamma}{\gamma-1}\theta+\frac{v^2}{2}\right)=a(r) \tag{13}$$

$$\theta(r)=0.232r^{2/3}, \qquad v(r)=1.077r^{1/3},$$

$$M(r\to\infty)=1.89=\left(\frac{5}{\gamma}\right)^{1/2}>1 \tag{14}$$

Solving these equations with respect to $\frac{dv}{dr}$ and $\frac{d\theta}{dr}$, we have

$$\frac{d\theta}{dr}=\frac{\gamma-1}{v\left(\gamma\theta-v^2\right)}\left[a(r)\left(\theta-v^2\right)+2\frac{\theta v^3}{r}\right] \tag{14}$$

$$\frac{dv}{dr}=\frac{(\gamma-1)a(r)-\frac{2\gamma\theta v}{r}}{\gamma\theta-v^2} \tag{15}$$

Clearly, the singularity arises at a point with the Mach number value $M=v/(\gamma\theta)^{1/2}$ equal to unity, where both $\frac{dv}{dr}$ and $\frac{d\theta}{dr}$ have a similar singular behavior (the expression $\frac{\gamma}{(\gamma-1)}\frac{d\theta}{dr}+v\frac{dv}{dr}=\frac{a}{v}$ has no singularity). In the pellet vicinity, the problem is almost flat and

$$\frac{d\theta}{dv}=\frac{\theta-v^2}{v} \tag{16}$$

This means that the velocity and temperature are proportional to one another $\theta=Bv$, and the flow is subsonic here. Neglecting dependence of a on α we obtain

$$v(r)=\sqrt{\frac{2(\gamma-1)}{\gamma B}\int_1^r a(r_*)dr_*+v_0} \tag{17}$$

$$\theta(r)=\sqrt{\frac{2B(\gamma-1)}{\gamma}\int_1^r a(r_*)dr_*+\theta_0} \tag{18}$$

At the pellet surface, the kinetic energy of the flow is much less than the thermal energy, and $v(1)$ and $\theta(1)$ are small compared to unity. The flow is insensitive to the precise values of v_0, θ_0, and the zero boundary conditions can be imposed. Far from the pellet, the asymptotic solution [7] is valid and for γ=7/5

The flux is supersonic at that distance, and it is necessary to pass through the M=1 point.

On the assumption that the solutions of (17) and (18) are valid up to the sonic point r=r_* , where

$$v_* = \left[\frac{(\gamma-1)r_* a(r_*)}{2}\right]^{1/3} = \sqrt{\gamma\theta_*} \qquad (20)$$

it is possible to estimate B and r_*

$$B = \left[2(\gamma-1)\int_1^{r_*} a(r)dr\right]^{1/3}\gamma^{-1} \qquad (21)$$

$$r_* a(r_*) = 4\int_1^{r_*} a(r)dr \qquad (22)$$

In the Milora assumption $a(r)$=1, we immediately have his result

$$r_* = \frac{4}{3}\ , \qquad B = \left[\frac{2}{3}(\gamma-1)\right]^{1/3}\gamma^{-1} = 0.46 \qquad (23)$$

For a more realistic $a(r)$-function corresponding to the Maxwellian energy flux deceleration

$$a(S_n) = exp\left(-\frac{S_n}{S_{n0}}5.94\right) \qquad (24)$$

the solutions of Eqs. (12) and (13) can be obtained numerically with the following boundary conditions: a_0=2.624×10^{-3} , T_0=0.015863 , v_0=0.042 , dN/dt=2×10^{23} 1/s, S_{n0}=2.2×10^{18} cm^{-2} , A=2.18×10^{-5} erg/s , V_0=6.885×10^5 cm/s.

The boundary velocity v_0 corresponds to the pellet temperature of 20 K. It was fixed in our simulations while the surface temperature T_0 and the optical thickness (or ablation rate) were determined by the two conditions: transition of the solution through the sonic point and $a(\infty)$=1. The results of the simulations are presented in Fig. 2.

It is seen that the dimensionless velocity $v(r)$ (curve 1) and temperature $\theta(r)$ (curve 2) tend to the corresponding asymptotic curves 3 and 4. The significant difference between the case $a(r)$=1, which is represented by curves 5, 6

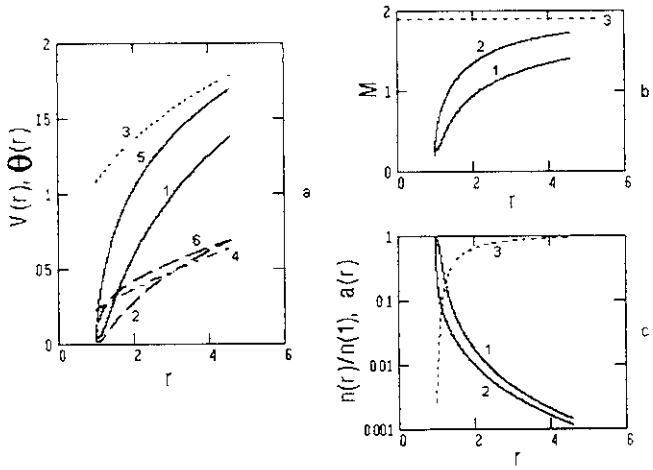

Figure 2: Gasdynamic parameters of the cloud. $a(S_n)$ is determined by Eq. (23). a)- dimensionless flow velocity and temperature versus radius; curves: 1- velocity, 2- temperature (numerical solution); 3- velocity, 4- temperature (asymptotic), 5- velocity, 6- temperature ($a(r)$=1 case). b)- Mach number; curves: 1- kinetic heating, 2- $a(r)$=1 case. c)- density profiles for kinetic heating (1) and $a(r)$=1 case (2), and the $a(r)$-function (3).

and our calculations is obvious. For kinetic model of heating, the growth of the Mach number goes on slower (compare curves 1 and 2 in Fig. 2 (b)). The gas density profile is mostly sensitive to the kinetic heating approach. In Fig. 2 (c) the profiles of $n(r)/n(1)$ are presented for the cases of uniform ($a(r)$=1) and kinetic model of heating as well as the function $a(r)$ corresponding to the kinetic model of heating. The density decreases slower for the kinetic heating case; at the sonic radius it is ~50 times less than at r=1, and the optical thickness is determined by the region very close to the pellet surface.

With the density profile $n(r)/n(1)$, which satisfies the set of Eqs. (14), (15) and (24), we obtain

$$S_n = \frac{\dfrac{dN}{dt}}{4\pi R_p V_0 v_0}\int_1^{\infty}\frac{n(r)}{n(1)}dr = \frac{4\pi R_p^2\dfrac{dR_p}{dt}2n_m}{4\pi R_p V_0 v_0}\int_1^{\infty}\frac{n(r)}{n(1)}dr \qquad (25)$$

and the scaling law for ablation is similar to the Milora and Foster law:

$$\frac{dR_p}{dt} = -\frac{v_0}{\int_1^\infty \frac{n(r)}{n(1)} dr} \frac{S_n}{2n_m R_p} \left(\frac{R_p}{m_i} \frac{dq}{dS_{n0}} \right)^{1/3} \quad (26)$$

The density profile integral is equal to 0.0597 for $a(S_n)$=1 and 0.1988 for our case. By changing the derivative in Eq. (26) by the ratio q/S_n, we arrive at the Milora form of the ablation scaling

$$\frac{dR_p}{dt} = -\frac{5.94^{1/3} \cdot v_0}{\int_1^\infty \frac{n(r)}{n(1)} dr} \frac{S_n}{2n_m R_p} \left(\frac{R_p}{m_i} \frac{q}{S_n} \right)^{1/3} = \quad (27)$$

$$-0.383 \frac{S_n}{2n_m R_p} \left(\frac{R_p}{m_i} \frac{q}{S_n} \right)^{1/3}$$

For the $a(S_n)$=1 case the coefficient is 0.704 instead of 0.383. The Milora scaling [7] corresponds to the numerical coefficient in Eq. (27) equal to 0.58. Thus our kinetic gas dynamics result (0.383) is equal to 0.66 of the Milora scaling or to 0.544 of that obtained here using uniform approach.

3 Analytic Approach to the 2-D Gasdynamic Ablation Problem

The zero boundary conditions at the pellet surface seem a reasonable approximation. The problem of the conditions at infinity is more complicated. The reason is associated with gradual increase of the secondary plasma density in the cloud and influence of the magnetic field on the cloud motion. An opinion exists that at a place where the ionization degree is considerable ("ionization radius"), the motion of the cloud across the magnetic field is stopped. The secondary plasma is spreading along the magnetic field [12]. The arising two-dimensional problem is very complicated. Numerous examples were analyzed in literature on MHD transformation of energy [2]. An additional obstacle consists in the fact that such a non-uniform flow of partially ionized plasma across the magnetic field with considerable probability is turbulent. Fortunately, significant ionization starts far away from the pellet surface (r>8-10) where the cloud density is small. Therefore, we restrict ourselves by the simplest model assuming the boundary conditions Eq. (19) azimuthally independent.

The co-ordinate system used in our analysis of the gas dynamic ablation problem is shown in Fig. 3. The z-axis is along the magnetic field B, the electron energy flux propagates in this direction. In the following analysis we neglect the angular fluxes in the cloud because the radial gradients are substantially greater than the angular ones in the region responsible for the optical thickness formation.

The optical thickness of the cloud at a point with the co-ordinates (P_0, z) or (α, R) is

$$S_n(z, P_0) = \int_z^\infty N(z', P_0) dz' \quad (28)$$

The density N at the point (z', P_0) is obviously

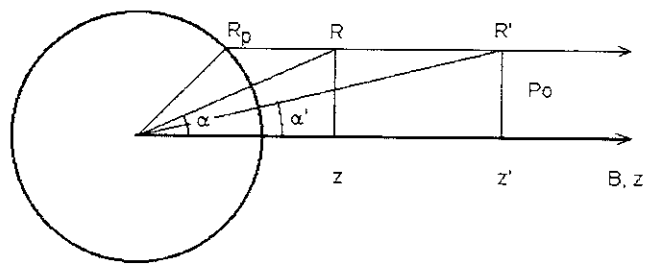

Figure 3: Co-ordinate system for analytical study of the gasdynamic scaling.

$$N(z', P_0) = \frac{G(\alpha')}{m_i R_p^2} \frac{R_p^2}{(R')^2 V(R', \alpha')} \quad (29)$$

where $\Gamma(\alpha) = \frac{G(\alpha)}{m_i R_p^2}$ is the density of the particle flux emitted from the pellet surface at a poloidal angle α. Besides,

$$\Gamma(\alpha) = \frac{q(\alpha, R_p)}{\lambda} \cos\alpha \quad (30)$$

where q is the electron energy flux density (see Eq. (4)) and λ is the molecular sublimation energy. Rewriting Eq. (4) in a form

$$\frac{d\tilde{q}}{ds} = -a(r, \alpha) \quad (31)$$

where $\tilde{q} = q/q_0$ is the dimensionless energy flux of electrons normalized by its value at infinity, and $s = AS_n/q_0$ is the dimensionless optical thickness. From the set of Eqs. (28)-

(31), an expression for the dimensionless optical thickness can be obtained

$$s(r,\alpha)=\frac{AR_p}{\lambda V_0}\int\limits_{z=R\cos\alpha}^{\infty}\frac{\tilde{q}(1,\alpha')\cos\alpha' dz'}{(r')^2 R_p v(r',\alpha')}= \frac{\overline{\chi}}{r\sin\alpha}\int\limits_0^{\alpha}\frac{\tilde{q}(1,\alpha')\cos\alpha' d\alpha'}{v\left(r'=r\frac{\sin\alpha}{\sin\alpha'},\alpha'\right)} \quad (32)$$

The parameter $\overline{\chi}=AR_p/\lambda V_0 >>1$ characterizes the ratio of the energy losses by the electron heat flux per molecule and the sublimation energy. It has the order of the shielding factor (q_0/q_1). A typical value for our conditions considered in Fig. 2 is $\overline{\chi}\cong 100$. The dimensionless heat flux on the pellet surface $\tilde{q}(1,\alpha)\equiv q_1(\alpha)=\tilde{q}(s(1,\alpha))$ is a function of the total optical length along the z'-axis from the point $(1,\alpha)$ to infinity. Substituting the velocity $v(r',\alpha')$ in accordance with Eqs. (11) and (17), we have

$$s(r,\alpha)=\frac{\chi}{r\sin\alpha}\int\limits_0^{\alpha}\frac{q_1(1,\alpha')\cos\alpha' d\alpha'}{\sqrt{\int\limits_1^{r'=r\sin\alpha/\sin\alpha'}a(r'',\alpha')dr''}} \quad (33)$$

where $\chi=\chi(\alpha)=\overline{\chi}\sqrt{\frac{\gamma B(\alpha)}{2(\gamma-1)}}$. It should be noted that $\tilde{q}(s)$ and $a(s)=-\frac{d\tilde{q}}{ds}$ strongly (exponentially) depend on s. Thus, it is more convenient to operate with the function $\phi(s)=-\ln(a(s))$, having the a- and q-functions redefined as follows:

$$a(s)=exp(-\phi(s)),\ \tilde{q}(s)=\int\limits_s^{\infty}exp(-\phi(s'))ds'$$

where $\phi(s)$ is a monotonously growing function of s, and $\phi(0)=0$.

Consider first the case $\alpha=0$, which corresponds to a region near the z-axis. From Eq. (33), it follows that

$$s(r,0)=\chi\int\limits_r^{\infty}\frac{q_1(s(1,0))dr'}{(r')^2\sqrt{\int\limits_1^{r'}exp(-\phi(r''))dr''}} \quad (34)$$

As the main shielding is governed by the zone close to the pellet surface, we omit the term $(r')^2$ in the denominator and get a derivative of the Eq. (25) over r. The result is

$$\frac{ds}{dr}=-\frac{\chi q_1}{\sqrt{\psi}}=-\frac{\chi}{\sqrt{\psi}}\int\limits_{s_1}^{\infty}exp(-\phi(s'))ds'$$
$$\frac{d\psi}{dr}=exp(-\phi(s)) \quad (35)$$

where $\psi(r)=\int\limits_1^{r}exp(-\phi(r'))dr'$. The set of Eqs. (35) does not contain explicitly dependencies on r. By dividing the last equation by the first one, we obtain

$$\frac{d\psi}{ds}=-\frac{exp(-\phi(s))\sqrt{\psi}}{\chi q_1} \quad (36)$$

with the boundary condition ($s_1=s(1,0)$ being the optical thickness at the pellet surface)

$$\psi(s=0)=\psi_1=\int\limits_{s(1)=s_1}^{s(\infty)=0}exp(-\phi(s'))\frac{dr'}{ds'}ds' \quad (37)$$

However, the last integral is divergent. This divergence arises from our neglecting the term $(r')^2$ in the denominator of Eq. (34). To avoid this difficulty, we should restrain the integration region by a zone $(r_0-1)\sim 1$, because most of the optical thickness is located close to the pellet surface. Then from Eqs. (36) and (37) we obtain

$$2\chi q_1\left(\sqrt{\psi_1}-\sqrt{\psi}\right)=\int\limits_0^{s}exp(-\phi(s'))ds'$$

and the equation

$$\psi(s)=\left[\frac{\int_s^{s_1} exp\left(-\phi\left(s'\right)\right)ds'}{2\chi q_1}\right]^2=\int_1^r exp\left(-\phi\left(s'\left(r'\right)\right)\right)dr' \tag{38}$$

determines the radial dependence of s(r). After differentiation of Eq. (38) over r, we have

$$\frac{ds}{dr}=-\frac{2\chi^2 q_1^2}{\int_s^{s_1} exp\left(-\phi\left(s'\right)\right)ds'} \tag{39}$$

and

$$2\chi^2(r-1)q_1^2=\int_s^{s_1} ds'\int_{s'}^{s_1} exp(-\phi(s''))ds''= \int_s^{s_1}(s'-s)exp(-\phi(s'))ds' \tag{40}$$

Substituting s=0 into the integral Eq. (40) and defining the boundary for the optical thickness region as r_0, we obtain an equation for the heat flux onto the pellet surface (or ablation rate density)

$$q_1(s_1)=\sqrt{\frac{\int_0^{s_1} s\,exp(-\phi(s))ds}{2(r_0-1)}}\frac{1}{\chi}=\int_{s_1}^{\infty} exp(-\phi(s))ds \tag{41}$$

The dependence of the heat flux on the r_0 is weak. Thus, we can define the boundary radius r_0 as 2 or r_*. If the dependence of ϕ on s is linear: $\phi(s)=s$, (this corresponds to our numerical analysis, Eq. (24)), the solution can be obtained as follows. Taking into account that χ>>1 (>100) and s_1>>1 (it equals to 6-8 in typical tokamak conditions), we have:

$$s_1=ln\left[\chi\sqrt{2(r_0-1)}\right]$$

$$\frac{r-1}{r_0-1}=exp(-s_1)\left[(exp(s_1-s)-1)-(s_1-s)\right]= \frac{exp(s_1-s)-1-(s_1-s)}{\chi\sqrt{2(r_0-1)}} \tag{42}$$

At the pellet surface $(s_1-s)\sim\sqrt{(r-1)\chi}$, while further the optical thickness varies by a logarithmic law $(s_1-s)\approx ln[\chi(r-1)]$. A half of the optical thickness is located within the region $(r-1)\le\chi^{-1/2}$.

Using Eq. (42) and the definitions of the functions, we come to the Milora-like form of the ablation scaling:

$$\frac{1}{\sqrt{\frac{\gamma}{\gamma-1}(r_0-1)B}}\frac{q_0\left(\frac{R_p}{m_i}\frac{dQ}{dS_{no}}\right)^{1/3}}{\frac{dq}{dS_{n0}}2n_m R_p}= \frac{1}{\sqrt{\frac{\gamma}{\gamma-1}(r_0-1)B}}\frac{S_n}{2n_m R_p}{}_0\left(\frac{R_p}{m_i}\frac{dQ}{dS_{no}}\right)^{1/3} \tag{43}$$

Assuming r_0=2 and B=2.5, we obtain the coefficient in the ablation scaling equal to

$\frac{5.94^{1/3}}{\sqrt{\frac{\gamma}{\gamma-1}(r_0-1)B}}=0.612$, which is only 50% greater than that (0.383) obtained numerically .

For the nonaxial case ($\alpha\neq0$), Eq. (33) can be written as follows:

$$s(r,\alpha)\approx\chi(\alpha)\int_r^{\infty}\frac{q_1(s_1(\alpha))cos^2\alpha dr'}{\sqrt{\int_1^{r'} a(r'',\alpha)dr''}} \tag{44}$$

It has the form of Eq. (34) with $\chi(0)$ replaced by $\chi(\alpha)\cos^2\alpha$ Its solution $s(1.\alpha)$ coincides with Eq (42) with the same substitution. It follows that the function $s(1.\alpha)$ is a weak (logarithmic) one of the angle α. If we neglect this dependence and assume $s(1,\alpha)\approx s_1$, and remember that the geometry is close to the flat one in the region determining the optical thickness, we obtain for the points not too close to $\alpha = \pi/2$:

$$\frac{dr_p}{dt} \sim \cos(\alpha) \tag{45}$$

This corresponds to cos-distribution of the ablation rate density over the pellet surface and to the lentil model considered in Ref. [10]. For a spherical pellet the ablation rate can be obtained simply by multiplying the ablation rate density, Eq. (43), by the doubled pellet cross-section area

$$\frac{dN}{dt} = 2\pi R_p^2 2n_m \frac{dR_p}{dt} \tag{46}$$

4 Ablation Rate Scaling

We see that the parameter dependencies of the kinetic gasdynamic scaling are the same as in the Milora analysis, except for the numerical coefficient, which is approximately two times less. Such a decrease only slightly affects the ablation scaling dependencies on the plasma parameters. A possible variation of the energy balance point is seen in Fig. 4.

Although the ablation scaling [10] remains valid, the numerical factor in it should be reduced by a factor of 0.6. Thus, we have

$$dN/dt = 2\times 10^{14} n_e^{0.453} T_e^{1.72} r_p^{1.443} M_i^{-0.283} \tag{47}$$

where n_e and T_e are the electron density (in cm^{-3}) and temperature (in eV), r_p is the pellet radius (in cm), M_i is mass of the pellet material in atomic units and dN/dt is in atom/s. After this variation, the kinetic "charged model" [10] practically agrees with the Parks scaling. The deviation of the lentil model [10] from the Parks scaling is not very large. Under the ITER conditions, the penetration lengths for the three models differ not greater than by 15 % (see Fig. 5).

The results presented show that a consideration of kinetic effects in a pellet cloud, which includes the energy flux modification, gas dynamics and two-dimensional effects, allows us to eliminate the discrepancy between the kinetic NGSM and the monoenergy model. Meanwhile, the

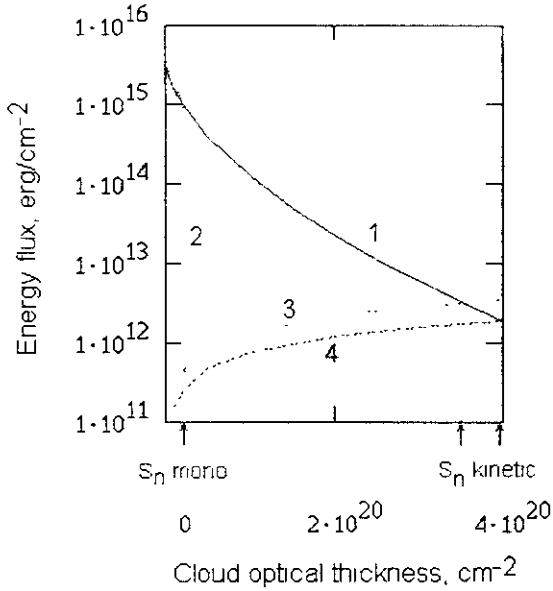

Figure 4: Energy fluxes versus the cloud optical thickness. The plasma parameters are as in Fig. 1. Curves: 1- kinetic electron energy flux; 2- monoenergy electron energy flux; 3- Milora gasdynamic scaling; 4- kinetic gasdynamic scaling. The balance optical thickness is 2.23×10^{19} cm^{-2} for the monoenergy approximation, 4×10^{20} cm^{-2} in our kinetic approach and 3.6×10^{20} cm^{-2} in the case considered in Ref. [10].

considerable changes in the cloud parameters must affect the previous estimations of plasma [3] and magnetic shielding [5,6]. As plasma shielding is a function of ablation rate, the estimations of the plasma cloud optical thickness based on monoenergy models are more or less correct (if cloud turbulence is insignificant [10]). However, even in this case, the increase of the neutral cloud optical thickness as compared to the monoenergy one (see Fig. 4, approximately 20 times!) makes the plasma shielding part relatively insignificant. A qualitatively similar situation refers to the magnetic shielding due to a significant decrease in the gas flow velocities and the respective reduction of expelling the magnetic field lines away from the pellet surface. A quantitative estimation of this effect is required, this task goes beyond of the purpose of this paper.

5 Summary

The problem of the cloud surrounding an ablating hydrogen pellet is treated using a kinetic two-dimensional approach. It is shown that the cloud is much thicker than in

the case of monoenergy electron heat flux. Nevertheless, the parameter dependencies of the ablation gasdynamic scaling are the same for kinetic and monoenergy approaches. Kinetic effects in the cloud gas dynamics reduce the pellet ablation rate and bring in good agreement the kinetic ablation models and the NGSM fairly well supported by contemporary tokamak experiments. The results can be used for the development of more sophisticated models accounting for detailed atomic processes in the cloud, and for estimations of plasma and magnetic shielding effects.

Acknowledgements

The authors are grateful to Prof. S. Sudo for his attention to the work and fruitful discussions.

References

[1] Gouge, M.J., Houlberg, W.A., Milora, S.L., Fusion Technol. **19** (1991) 95.

[2] Milora, S.L., Houlberg, W.A., Lengyel, L.L., Mertens, V., Nucl. Fusion, **35** (1995) 657.

[3] Kaufmann, M., Lackner, K., Lengyel, L.L., et al., Nucl. Fusion **26** (1986) 171.

[4] Rozhansky, V.A., Sov. J. Plasma Physics **15** (1989) 638.

[5] Parks, P.B., Nucl. Fusion **20** (1980) 311.

[6] Lengyel, L.L., Nucl. Fusion **29** (1989) 37.

[7] Milora, S.L., Foster, C.A., IEEE Trans. Plasma Sci. **PS-6** (1978) 578.

[8] Parks, P.B., Turnbull, R.J., Phys. Fluids **21** (1978) 1735.

[9] Houlberg, W.A., Attenberger, S.E., Baylor, L.R., et al., Nucl. Fusion **32** (1992) 1951.

[10] Kuteev, B.V., "Pellet ablation in the Large Helical Device", NIFS-260 report, Nagoya, Japan, Nov. 1993, Kuteev, B.V. Nucl. Fusion **35** (1995) 431.

[11] Macaulay, A.K., Nucl. Fusion **34** (1994) 43.

[12] Lengyel, L.L., Spathis P.N., Nucl. Fusion 34 (1994) 675.

[13] Spathis, P.N., Lengyel, L.L., in 1992 International Coonference on Plasma Physics (Proc. Conf. Innsbruck, 1992), Vol. 16C, Part I, European Physical Society, Geneva (1992) 323.

[14] Spathis, P.N., Field Aligned Expantion of Particle Clouds in Magnetically Confined Plasmas, Tech. Rep. IPP 5/38, Max-Plank-Institut für Plasmaphysik, Garching (1992).

[15] Kuteev, B.V., Umov, A.P., Tsendin, L.D., Sov. J. Plasma Phys. **11** (1985) 236.

[16] Baylor, L.R., et al., Nucl. Fusion (IPADBASE) submitted to publication.

[17] Kuteev, B.V., et al., Abstracts of the Eleventh Topical Meeting on the Technology of Fusion Energy. June 19-23, 1994, New Orleans, Louisiana. ANS, Inc., La Grange Park, Illinois, (1994), p.327.

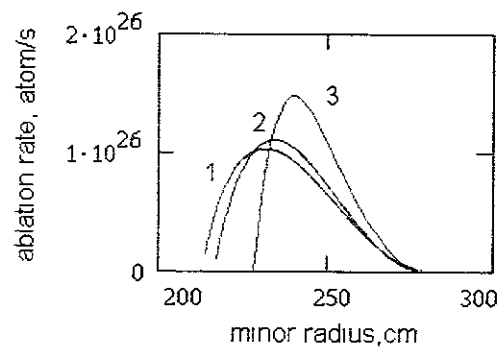

Figure 5: Deuterium pellet penetration into ITER. r_p=0.5 cm, v_p=1200 m/s, $n(r)=2\times10^{14}(1-(r/a_L)^2)^{0.5}$ cm^{-3}, $T_e(r)=14000(1-(r/a_L)^2)$ eV, a_L=280 cm is the minor tokamak radius.
Curves: 1- Parks' ablation scaling, 2- charged model, 3- lentil model. The last two curves are obtained from the ablation scaling Eq. (46).

Recent Issues of NIFS Series

NIFS-692 K Ichiguchi, T Nishimura, N Nakajima, M Okamoto, S -I Ohkawa, M Itagaki,
Effects of Net Toroidal Current Profile on Mercier Criterion in Heliotron Plasma, Apr 2001

NIFS-693 W Pei, R Horiuchi and T Sato
Long Time Scale Evolution of Collisionless Driven Reconnection in a Two-Dimensional Open System, Apr 2001

NIFS-694 L N Vyacheslavov, K Tanaka, K Kawahata
CO2 Laser Diagnostics for Measurements of the Plasma Density Profile and Plasma Density Fluctuations on LHD, Apr 2001

NIFS-695 T Ohkawa,
Spin Dependent Transport in Magnetically Confined Plasma, May 2001

NIFS-696 M Yokoyama, K Ida, H Sanuki, K Itoh, K Narihara, K Tanaka, K Kawahata, N Ohyabu and LHD experimental group
Analysis of Radial Electric Field in LHD towards Improved Confinement, May 2001

NIFS-697 M Yokoyama, K Itoh, S Okamura, K Matsuoka, S -I Itoh,
Maximum-J Capability in a Quasi-Axisymmetric Stellarator, May 2001

NIFS-698 S-I Itoh and K Itoh,
Transition in Multiple-scale-lengths Turbulence in Plasmas, May 2001

NIFS-699 K Ohi, H Naitou, Y Tauchi, O Fukumasa,
Bifurcation in Asymmetric Plasma Divided by a Magnetic Filter, May 2001

NIFS-700 H Miura, T Hayashi and T Sato
Nonlinear Simulation of Resistive Ballooning Modes in Large Helical Device, June 2001

NIFS-701 G Kawahara and S Kida,
A Periodic Motion Embedded in Plane Couette Turbulence, June 2001

NIFS-702 K Ohkubo,
Hybrid Modes in a Square Corrugated Waveguide, June 2001

NIFS-703 S -I Itoh and K Itoh
Statistical Theory and Transition in Multiple-scale-lengths Turbulence in Plasmas, June 2001

NIFS-704 S Toda and K Itoh,
Theoretical Study of Structure of Electric Field in Helical Toroidal Plasmas, June 2001

NIFS-705 K Itoh and S-I Itoh,
Geometry Changes Transient Transport in Plasmas, June 2001

NIFS-706 M Tanaka and A Yu Grosberg
Electrophoresis of Charge Inverted Macroion Complex Molecular Dynamics Study: July 2001

NIFS-707 T-H Watanave, H Sugama and T Sato
A Nondissipative Simulation Method for the Drift Kinetic Equation, July 2001

NIFS-708 N Ishihara and S Kida,
Dynamo Mechanism in a Rotating Spherical Shell: Competition between Magnetic Field and Convection Vortices, July 2001

NIFS-709 LHD Experimental Group,
Contributions to 28th European Physical Society Conference on Controlled Fusion and Plasma Physics (Madeira Tecnopolo, Funchal, Portugal, 18-22 June 2001) from LHD Experiment, July 2001

NIFS-710 V Yu Sergeev, R K Janev, M J Rakovic, S Zou, N Tamura, K V Khlopenkov and S Sudo
Optimization of the Visible CXRS Measurements of TESPEL Diagnostics in LHD, Aug 2001

NIFS-711 M Bacal, M Nishiura, M Sasao, M Wada, M Hamabe, H Yamaoka,
Effect of Argon Additive in Negative Hydrogen Ion Sources, Aug 2001

NIFS-712 K Saito, R Kumazawa, T Mutoh, T Seki, T Watari, T Yamamoto, Y Torii, N Takeuchi, C Zhang, Y Zhao, A Fukuyama, F Shimpo, G Nomura, M Yokota, A Kato, M Sasao, M Isobe, A V. Krasilnikov, T Ozaki, M Osakabe, K. Narihara, Y Nagayama, S Inagaki, K Itoh, T Ido, S Morita, K Ohkubo, M Sato, S Kubo, T Shimozuma, H Idei, Y Yoshimura, T Notake, O Kaneko, Y Takeiri, Y Oka, K. Tsumori, K Ikeda, A Komori, H Yamada, H Funaba, K Y Watanabe, S Sakakibara, R Sakamoto, J Miyazawa, K Tanaka, B J. Peterson, N Ashikawa, S Murakami, T Minami, M Shoji, S Ohdachi, S Yamamoto, H Suzuki, K Kawahata, M Emoto, H Nakanishi, N Inoue, N Ohyabu, Y Nakamura, S Masuzaki, S Muto, K Sato, T Morisaki, M Yokoyama, T Watanabe, M Goto, I Yamada, K Ida, T Tokuzawa, N Noda, K Toi, S Yamaguchi, K Akaishi, A Sagara, K Nishimura, K Yamazaki, S Sudo, Y Hamada, O Motojima, M Fujiwara,
A Study of High-Energy Ions Produced by ICRF Heating in LHD, Sep 2001

NIFS-713 Y Matsumoto, S -I Ohkawa and T Watanabe,
Field Line and Particle Orbit Analysis in the Periphery of the Large Helical Device, Sep 2001

NIFS-714 S. Toda, M Kawasaki, N Kasuya, K Itoh, Y. Takase, A Furuya, M Yagi and S -I Itoh,
Contributions to the 8th IAEA Technical Committee Meeting on H-Mode Physics and Transport Barriers (5-7 September 2001, Toki, Japan) Oct 2001

NIFS-715 A Maluckov, N Nakajima, M Okamoto, S Murakami and R. Kanno,
Statistical Properties of the Particle Radial Diffusion in a Radially Bounded Irregular Magnetic Field, Oct 2001

NIFS-716 Boris V. Kuteev
Kinetic Depletion Model for Pellet Ablation, Nov 2001

NIFS-717 Boris V Kuteev, Lev D Tsendin,
Analytical Model of Neutral Gas Shielding for Hydrogen Pellet Ablation, Nov 2001

Printed on 100% Recycled Paper for this Text